postulated that if neuronal cell loss in the substantia nigra is associated with age-related DAT decline in the striatum, the regional distribution of cell loss in the substantia nigra should be associated with the regional distribution of age-related DAT decline in the striatum. This is because cells in the substantia nigra project to the striatum with a regionally corresponding arrangement. Further, if age-related DAT decline is associated functionally with age-related D_2R decline, the regional distribution of the age-related decreasing rate of DATs should be associated with that of D_2Rs in the striatum, because presynaptic terminals are adjacent to postsynaptic neurons.

To examine this hypothesis, we focused on investigating the regional difference in the age-related deceasing rates. We divided the striatum into three regions-caudate nucleus, anterior putamen, and posterior putamen. We then investigated the age-related changes and the association between DATs and D_2Rs for each region in the same subject by PET. Additionally, to visually evaluate the detailed regional differences in the deceasing rate of each marker, we developed a new imaging technique to create a decay image that maps the slope of the regression line on a voxel-by-voxel basis.

MATERIALS AND METHODS

Subjects

A total of 16 healthy volunteers (15 men and 3 women), ages 21–74 years (mean age = 42.3, SD = 21.1), participated in this study. All subjects were right-handed. They were deemed healthy based on their medical history, physical and neurological examinations by neurologists, and magnetic resonance imaging (MRI) of the brain evaluated by radiologists. None of them was on medication at the time of the study. This study protocol was approved by the Ethics Committee of the Tokyo Metropolitan Institute of Gerontology. Written informed consent was obtained from all participants.

PET imaging

PET studies were performed at the Positron Medical Center, Tokyo Metropolitan Institute of Gerontology using a SET 2400W scanner (Shimadzu, Kyoto, Japan) in the three-dimensional scanning mode (Fujiwara et al., 1997). Carbon-11-labeled 2β-carbomethoxy-3β-(4-fluorophenyl)-tropane ([^{11}C]CFT) and Carbon-11-labeled raclopride ([^{11}C]raclopride) were prepared as described previously (Kawamura et al., 2003; Langer O, 1999). All subjects underwent the two PET studies on the same day. Each subject received an intravenous bolus injection of 352 ± 49 (mean ± SD) MBq of [^{11}C]CFT. Then, 2.5–3 h after the injection of [^{11}C]CFT, each subject received an intravenous bolus injection of 322 ± 48 (mean ± SD) MBq of [^{11}C]raclopride. To estimate the binding potentials, for 5 of 16 subjects, dynamic scans were performed for 90 min with [^{11}C]CFT and for 60 min with [^{11}C]raclopride. To measure the uptake of these two tracers, for the remaining 11 subjects, static scans were performed for 75–90 min after the injection of [^{11}C]CFT and for 40–55 min after the injection of [^{11}C]raclopride, respectively. The specific activity at the time of injection ranged from 12.4 to 119.6 GBq/μmol for [^{11}C]CFT and from 14.0 to 188.0 GBq/μmol for [^{11}C]raclopride. The transmission data were acquired using a rotating ^{68}Ga/^{68}Ge rod source for attenuation correction. The images consist of 2 × 2 × 3.125 mm^3 voxels with a 128 × 128 matrix and 50 slices.

MR imaging

High-resolution MRI was obtained using a 1.5-Tesla Sigma EXCITE HD scanner (GE, Milwaukee, WI) in the three-dimensional mode (3DSPGR; echo time: 2.3 ms, repetition time: 18 ms), which provided 124 contiguous slices with a matrix size of 256 × 256, pixel size of 0.9375 × 0.9375 mm^2, and slice thickness of 1.3 mm.

Data analysis

Uptake ratio index on region-of-interest basis

Image manipulations were carried out by using a medical image processing application package "Dr View/LINUX" version R2.0 (AJS, Tokyo, Japan) and SPM2 (The Wellcome Department of Imaging Neuroscience, Institute of Neurology, University College London, London, UK) implemented in MATLAB version 7.0.1 (MathWorks,. Natick, MA).

Circular regions of interest (ROIs) were placed with reference to the brain atlas and individually coregistered MRI by SPM2: one region of interest (ROI) with 6-mm diameter was placed on the caudate, two ROIs on the anterior putamen and two ROIs on the posterior putamen to contain the most intense activity on both the left and right sides in each of the two contiguous slices. Each ROI in the striatum was estimated smaller enough based on the actual structure of MRI to minimize resolution-induced problem with ill-defined edges. A total of 50 ROIs with 10-mm diameter were placed throughout the cerebellar cortex in five contiguous slices.

To evaluate the uptake of [^{11}C]CFT and [^{11}C]raclopride, we calculated the uptake ratio index by the following formula (Antonini et al., 1993; Frost et al., 1993; Wong et al., 1993).

$$\text{Uptake Ratio Index} = \frac{(\text{Activity}_{\text{Region}} - \text{Activity}_{\text{Cerebellum}})}{\text{Activity}_{\text{Cerebellum}}}$$

Individual uptake ratio index was calculated not only for the static scanned 11 subjects but also for the dynamic scanned five subjects using the data obtained from an equivalent time-frame.

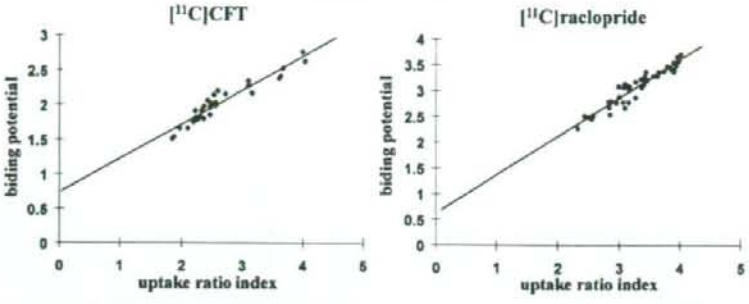

Fig. 1. Correlations between the binding potentials and uptake ratio indexes for [^{11}C]CFT (left) and [^{11}C]raclopride (right) in the striatum. Solid lines represent the regression lines. Linear correlation was significant for [^{11}C]CFT ($r = 0.95$; $P < 0.001$) and [^{11}C]raclopride ($r = 0.95$; $P < 0.001$).

Uptake ratio index and binding potential

To validate adopting the uptake ratio index, we examined the correlation between the binding potential (BP) and the uptake ratio index. Six ROIs were placed on the striatum of each dynamic scanned subject. The BP of each ROI for each tracer was estimated by a simplified reference region model using the cerebellum as a reference (Gunn et al., 1997). The cerebellum was selected as a reference region in the analysis, because it contains negligible levels of DATs, and D_2Rs. The uptake ratio index of each ROI was also estimated, as described earlier. Then, we compared the BPs of total 30 ROIs with the uptake ratio indexes of those.

Image processing of age-related decline on a voxel-by-voxel basis

To acquire the voxel-by-voxel regression images representing the slope of decline, we used SPM2 for the anatomical standardization and coregistration of the image. Individual [^{11}C]CFT and [^{11}C]raclopride uptake index images normalized to cerebellar activity, as described earlier, and MRI images were coregistered. Then, individual [^{11}C]CFT uptake index images were anatomically transformed into standard brain images using the in-house-developed [^{11}C]CFT image template, which was built in accordance with the strategy descried elsewhere (Meyer et al., 1999). The same transformation parameters were applied to the individual coregistered [^{11}C]raclopride uptake index images and MRI images. Additionally, we obtained the average MRI image from the transformed MRI images of 16 subjects.

To evaluate visually and statistically the regional differences in the aging effect within the striatum, we developed a software that could perform a linear regression analysis on a voxel-by-voxel basis between the age and uptake ratio index of [^{11}C]CFT and [^{11}C]raclopride. We also created parametric images mapping the slope of the regression line and the correlation coefficient (r) for each tracer. We called the former images age-related slope-of-decline images. We clipped the voxels with significant decline ($P < 0.01$) from the new images and superimposed them on the average MRI of 16 subjects.

Statistics

ROI-based analyses were performed by using the average of the right and the left uptake ratio indexes because of the following reasons. First, for each subregion of each tracer, neither the two-tailed paired *t*-test with Bonferroni correction nor analysis of variance with Levene's test revealed significant correlation between the right and the left uptake ratio indexes. Second, for each subregion of each tracer, the left-right difference in regression slope between the age and uptake ratio indexes was not statistically significant by using analysis of covariance. All statistical analyses were performed by using the software package JMP version 5.1.1 (SAS Institute, Cary, NC). *P* values less than 0.01 were considered to be statistically significant.

RESULTS

There were significant positive liner correlations between the BP and the uptake ratio index for both [^{11}C]CFT ($r = 0.95$; $P < 0.001$) and [^{11}C]raclopride ($r = 0.95$; $P < 0.001$), as shown in Figure 1. Therefore, we adopted the uptake ratio index for the further analysis.

ROI-based regression analysis revealed a highly significant age-related linear decline in the uptake ratio index of [^{11}C]CFT in the caudate nucleus ($r = 0.84$; $P < 0.001$), anterior putamen ($r = 0.75$; $P < 0.001$), and posterior putamen ($r = 0.79$; $P < 0.001$), and in that of [^{11}C]raclopride in the caudate nucleus ($r = 0.81$; $P < 0.001$), anterior putamen ($r = 0.80$;

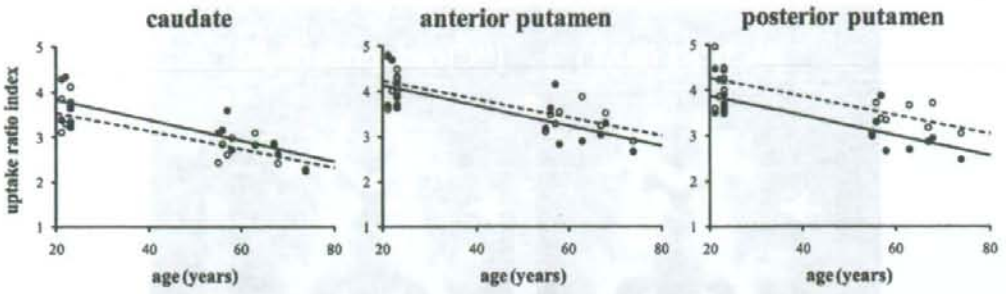

Fig. 2. Correlations between the age and uptake ratio indexes for [^{11}C]CFT (filled circles) and [^{11}C]raclopride (open circles) in the caudate (left), anterior putamen (middle), and posterior putamen (right). Solid lines represent the regression lines for [^{11}C]CFT and dotted lines, those for [^{11}C]raclopride. Linear correlation was significant for [^{11}C]CFT in the caudate ($r = 0.84$; $P < 0.001$), anterior putamen ($r = 0.75$; $P < 0.001$), and posterior putamen ($r = 0.79$; $P < 0.001$), and for [^{11}C]raclopride in the caudate nucleus ($r = 0.81$; $P < 0.001$), anterior putamen ($r = 0.80$; $P < 0.001$), and posterior putamen ($r = 0.77$; $P < 0.001$).

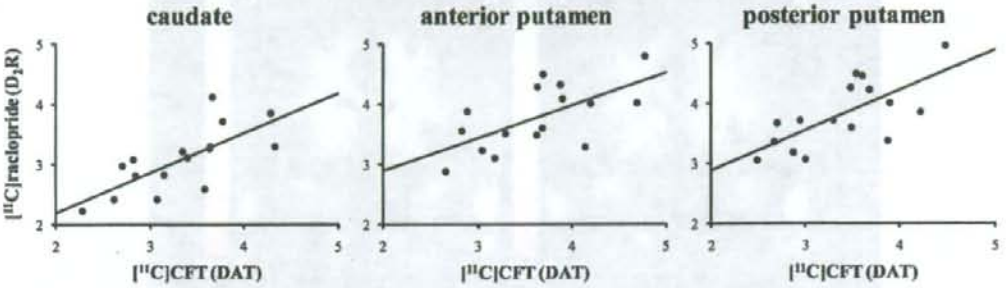

Fig. 3. Correlations between the uptake ratio indexes for [^{11}C]CFT and [^{11}C]raclopride in the caudate (left), anterior putamen (middle), and posterior putamen (right). Solid lines represent the regression lines. Linear correlation was significant for the caudate ($r = 0.73$; $P = 0.001$), anterior putamen ($r = 0.64$; $P = 0.008$), and posterior putamen ($r = 0.70$; $P = 0.003$).

$P < 0.001$), and posterior putamen ($r = 0.77$; $P < 0.001$), as shown in Figure 2. This decline corresponded to 6.1, 5.5, and 5.6% reduction per decade for [^{11}C]CFT uptake in the caudate nucleus, anterior putamen, and posterior putamen, respectively, and 5.8, 4.9, and 4.8% reduction per decade for [^{11}C]raclopride uptake in the caudate nucleus, anterior putamen, and posterior putamen. The [^{11}C]raclopride uptake was significantly correlated with the [^{11}C]CFT uptake in the caudate nucleus ($r = 0.73$; $P = 0.001$), anterior putamen ($r = 0.64$; $P = 0.008$), and posterior putamen ($r = 0.70$; $P = 0.003$), irrespective of age (Fig. 3).

For both [^{11}C]CFT and [^{11}C]raclopride, the age-related slope-of-decline images in Figure 4 showed that the significant decline was almost comparable to the results of ROI-based analysis, and we confirmed that most voxels in the striatum were included in the images. The decline rates in the caudate nucleus tended to be slightly higher than those in the subdivisions of the putamen. The difference between the decline rates in the anterior and posterior putamen was not obvious in both images. Moreover, two age-related slope-of-decline images were almost the same. Briefly, voxels with a high slope of decline in the age-related slope-of-decline image for [^{11}C]CFT also had a high slope of decline in the images for [^{11}C]raclopride. On the other hand, voxels with a low slope of decline in the images for [^{11}C]CFT also had a low slope of decline in the images for [^{11}C]raclopride. And although in ROI-based analysis there was no left-right statistically significant difference, in the image (shown in Finger 4) the decline rates in the left side tended to be higher than those in the right side in the striatum.

DISCUSSION

In this study, we simultaneously investigated the age-related change in DAT density and D_2R density, by particularly focusing on the regional difference. In addition to a conventional ROI-based analysis, in

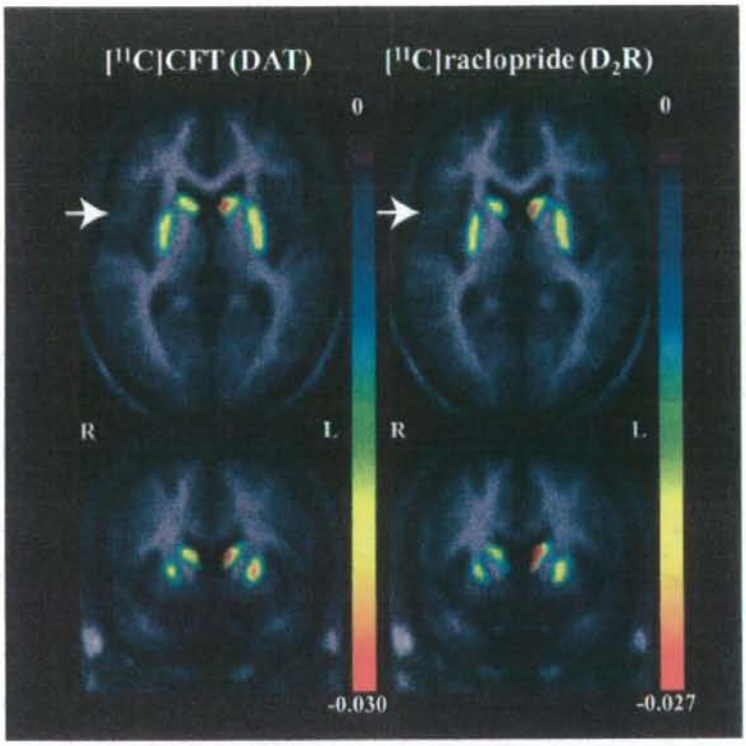

Fig. 4. The age-related slope-of-decline images superimposed on MRI for [^{11}C]CFT (left) and [^{11}C]raclopride (right) in transversal planes (top) at the level of the basal ganglia, and coronal planes (bottom) at the level of the white arrows marked in transversal planes. Voxels with significant decline ($P < 0.01$) were superimposed on MRI images. The degree of color scale represents the slope of the regression line between the age and uptake ratio index of each tracer on a voxel-by-voxel basis in the striatum and the scale value of −0.010 is equivalent to 2.6% reduction per decade. The images show the age-related regional rate of decline.

which the striatum was divided into three regions, we developed a novel method to create images mapping the slope of decline on a voxel-by-voxel basis so that we could investigate in detail the regional difference within the striatum in the aging effect on the nigrostriatal dopaminergic system. These images are equivalent to those made by visualizing the slope of the regression line between the age and uptake ratio index obtained by placing ROIs on every voxel. This new imaging technique superimposed on MRI can provide anatomical information in detail with high objectivity. This technique also completely eliminates arbitrariness and subjective elements, both of which are disadvantages of conventional ROI-based analysis. By reconfirming the result of the ROI-based analysis with the new imaging technique, the reliability of the research greatly improved. A possible limitation of this method is that the caudate nucleus could be influenced by the individual size of the lateral ventricles in the process of spatial normalization performed by SPM methods (Reig et al., 2007). Therefore, the caudate nucleus adjacent to the ventricles should be assessed carefully. Also, we should consider that the edge of the actual structure is susceptible to partial volume effects derived from original PET images.

In the process of creating the new imaging, the main problem was which template we should use for spatial normalization, because the use of different normalization strategies may alter noticeably the SPM map (Gispert et al., 2003). Two approaches to spatial normalization were considered. First was the ligand template approach, which was used in this study. Second was the MRI template approach: the coregistered MRI images to the PET images were spatially normalized to the SPM MRI template and the same transformations were applied to the PET images. On the basis of the study by Meyer et al.

TABLE I. In vivo human data: Age-related changes of dopamine transporter (DAT) and dopamine D_2-like receptor (D_2R)

In vivo	Name	Year	Type	Ligand	*n*	Age range (years)	Decreasing rate (% per decade)	Site
DAT	van Dyck et al.	1994	SPECT	[^{123}I]βCIT	28	18–83	8.0	Striatum
	Volkow et al.	1994	PET	[^{11}C]Cocaine	26	21–63	7.0	Striatum
	Ishikawa et al.	1996	SPECT	[^{123}I]βCIT-FP	15	45.5 ± 22.1[a]	3.3	Striatum
							6.4	Putamen
	Volkow et al.	1996a	PET	[^{11}C]d-Threo-methyphenidate	23	20–74	6.6	Striatum
	Kazumta et al.	1998	PET	[^{18}F]FPCIT	7	23–73	7.7	Caudate
							6.4	Putamen
	Rinne et al.	1998	PET	[^{11}C]βCFT	9	23–70	4.7	Caudate
							4.4	Putamen
	Volkow et al.	1998	PET	[^{11}C]d-Threo-methyphenidate	21	24–86	5[b]	Striatum
	Pirker et al.	2000	SPECT	[^{123}I]βCIT	16	21–75	6.6	Striatum
	Present data	2008	PET	[^{11}C]CFT	16	21–74	6.1	Caudate
							5.5	Anterior putamen
							5.6	Posterior putamen
D_2R	Wong et al.	1988	PET	[^{11}C]NMSP	36	19–71	8.3	Caudate
	Rinne et al.	1993	PET	[^{11}C]Raclopride	21	20–81	4.6	Striatum
	Volkow et al.	1996b	PET	[^{11}C]Raclopride	24	24–73	7.9	Striatum
	Wong et al.	1997	PET	[^{11}C]NMSP	24	13–79	8.4	Caudate
	Pohjlinen et al.	1998	PET	[^{11}C]Raclopride	54	19–82	5.0	Right striatum
							4.0	Left striatum
	Volkow et al.	1998	PET	[^{11}C]Raclopride	21	24–86	5[b]	Striatum
	Present data	2008	PET	[^{11}C]Raclopride	16	21–74	5.8	Caudate
							4.9	Anterior putamen
							4.8	Posterior putamen

[a]Mean ± SD.
[b]Estimated by us with the chart in original article.

TABLE II. In vitro post-mortem human data: Age-related changes of dopamine transporter (DAT) and dopamine D_2-like receptor (D_2R)

In vitro	Name	Year	Ligand	*n*	Age range (years)	Decreasing rate (% per decade)	Site
DAT	Zelnik et al.	1986	[^{3}H]GBR-12935	13	0–82	9[a]	Caudate
	Allard et al.	1989	[^{3}H]GBR-12935	20	19–100	8.8	Putamen
	De Keyser et al.	1990	[^{3}H]GBR-12935	32	19–88	9[a]	Putamen
D_2R	Severson et al.	1982	[^{3}H]Spiroperon	44	2–94	2.5	Caudate
			[^{3}H]ADTN			7.5	Caudate
	Rinne et al.	1987	[^{3}H]Spiroperidol	78	4–93	6.3	Putamen
	Seeman et al.	1987	[^{3}H]Spiroperon	247	0–94	2.2	Striatum
	Rinne et al.	1990	[^{3}H]Spiroperidol	65	6–93	3.8	Caudate
						3.7	Putamen

[a]Estimated by us with the chart in original article.

(1999), in which they suggested that the ligand template method provides a more reliable approach for spatial normalization of PET ligand-receptor images than the MRI template method, we chose the [^{11}C]CFT ligand template approach.

On the basis of the findings obtained from ROI-based analysis and the new imaging technique, we verified our hypothesis. In the ROI-based analysis, DAT density measured by [^{11}C]CFT PET was lost at rates of 6.1, 5.5, and 5.6% per decade in the caudate nucleus, anterior putamen, and posterior putamen, respectively. The corresponding rates for D_2R density measured by [^{11}C]raclopride PET were 5.8, 4.9, and 4.8% per decade, respectively. These results were comparable to previous neuroimaging studies that have shown the linear decline in DAT density ranging from 3.3 to 8.0% per decade (Ishikawa et al., 1996; Kazumata et al., 1998; Pirker et al., 2000; Rinne et al., 1998; van Dyck et al., 1995; Volkow et al., 1994, 1996a, 1998) and in D_2R density ranging from 4.6 to 8.4% (Pohjalainen et al., 1998; Rinne et al., 1993; Volkow et al., 1996b, 1998; Wong et al., 1988, 1997), as shown Table I. Despite sampling and methodological differences, previous in vitro postmortem studies using ligand binding techniques have also shown a significant age-related decline in DAT density (Allard and Marcusson, 1989; De Keyser et al., 1990; Zelnik et al., 1986) and D_2R density (Rinne, 1987; Rinne et al., 1990; Seeman et al., 1987; Severson et al., 1982), as shown Table II. In this study, the decline rates for both DAT and D_2R densities in the caudate nucleus were slightly higher than those in the putamen, as in the previous studies (Kazumata et al., 1998; Rinne et al., 1990, 1998). Meanwhile, the

decline rates for both DATs and D_2Rs in the anterior and posterior putamen were approximately the same. By using the age-related slope-of-decline images, we could reaffirm these tendencies.

However, despite of no left-right statistically significant deference in ROI-based analysis, the left side tended to be higher rate than the right side in the age-related slope-of-decline images. This might be because we placed relatively-small ROIs on the striatum to minimize partial volume effects. Actually small regions which include voxel with higher decreasing rate might be investigated preferentially. But with the age-related slope-of-decline images we could recognize the tendency by viewing the striatum macroscopically. Asymmetries of human cerebral functions have been revealed by neuroanatomy and neuroimaging studies (Laakso et al., 2000; Larisch et al., 1998; Toga and Thompson, 2003; Volkow et al., 1996a). There is also evidence from an animal study and a human study that the dopamine receptor asymmetry decreases with age (Giardino, 1996; Vernaleken et al., 2007). They indicated that the loss of asymmetry during normal aging may cause the left-right difference in the decreasing rate.

It has been confirmed that with an increase in age, neuronal loss occurs at a rate of 4.7–6.0% per decade in the substantia nigra (Fearnley and Lees, 1991; Gibb and Lees, 1991). Interestingly, this rate is almost same as the decline rate in DATs. The regional pattern of cell loss in the substantia nigra under normal aging is likely to preferentially affect the heavily pigmented neurons that are situated in the dorsomedial part of the substantia nigra (Gibb and Lees, 1991), an area where neuronal cells project preferentially to the caudate nucleus (Szabo, 1980). Our result, that the decline rate of DATs in the caudate nucleus was the fastest within the striatum, agreed with previous pathological studies. These findings indicate that the neuronal loss in the substantia nigra is strongly related to a significant decline of DATs during normal aging, and this supports our hypothesis. In other words, a decrease in DATs is likely to preferentially reflect neuronal loss in the substantia nigra.

In terms of the association between DATs and D_2Rs, our ROI-based analysis has shown significant correlation, irrespective of age in all three regions of the striatum. These results are comparable to those reported by Volkow et al. (1998). They evaluated DAT and D_2R densities by PET using [^{11}C]methylphenidate and [^{11}C]raclopride, respectively. They showed that DAT and D_2R densities decreased with age and that the association between DATs and D_2Rs was independent of age. And they suggested that a common mechanism regulates the expression of receptors and transporters. Furthermore, with the age-related slope-of-decline images, we could understand that the tendency of gradient distribution of the decreasing rate of DATs is almost same as that of D_2Rs throughout the striatum, not only along with the antero-posterior direction, but also along the ventro-dorsal and medio-lateral directions. These findings also supported our hypothesis. In other words, our results, in addition to the results presented by Volkow et al. (1998), suggested that a decrease in D_2Rs is likely to preferentially reflect the functional change in presynaptic and postsynaptic neurons, rather than neuronal loss in the striatum.

But actually the uptake of [^{11}C]raclopride reflects the total amount of dopamine D_2-like receptors, which include dopamine D_2, D_3, and D_4 receptor. Dopamine D_2 receptor has two isoforms, D_2L and D_2S, by a mechanism of alternative splicing (Picetti et al., 1997). D_2L acts mainly at postsynaptic sites and D_2S serves presynaptic autoreceptor functions (L'Hirondel et al., 1998; Mercuri et al., 1997). Therefore, the uptake of [^{11}C]raclopride could reflect presynaptic function corresponding to D_2 autoreceptor to some degree. But D_2S is less abundant than D_2L in the striatum (Giros et al., 1989; Guivarc'h et al., 1995; Monsma et al., 1989) and numerous D_2R imaging studies for parkinsonian disorders have indicated no discrepancy in the assumption that D_2R imaging could show mainly postsynaptic function (Piccini and Whone, 2004; Thobois et al., 2004). Then, we considered that the uptake of [^{11}C]raclopride reflects mainly postsynaptic function.

Considering our results, we could speculate that the age-related neuronal loss in the substantia nigra may trigger the structural change of presynaptic neurons (loss of DATs) in the striatum and this change may result in the functional change of postsynaptic neurons (loss of D_2Rs) in the striatum. Of course, the structural change of presynaptic neurons should also provoke the functional change of presynaptic neurons.

These functional changes include several presynaptic processes such as neurotransmitter synthesis, storage, metabolism, release, and reuptake/uptake, and postsynaptic processes such as receptor functioning, metabolism, and interactions with other neuromodulators (Reeves et al., 2002; Stanford et al., 2001). Functional changes such as the decrease in DAT mRNA (Bannon and Whitty, 1997) and changes in D_2R posttranscriptional regulation in striatal neurons (Sakata et al., 1992) have been reported.

The numbers of neurons and D_2R-containing cells in striatum also decrease during normal aging (Han et al., 1989; Meng et al., 1999); however, there exist no detailed histological reports on the regional differences in the decreasing rate. Future histological studies evaluating detailed regional differences in age-related decline of the numbers of D_2R-containing cells in the striatum are required. Such studies will help

to clarify the existence or nonexistence of the association between D_2R decline and cell loss in the striatum with aging. If such an association does not exist, our hypothesis will be supported more strongly.

In conclusion, we confirmed age-related decline in the striatal DAT and D_2R densities in normal subjects by conventional ROI-based analysis and by using age-related slope-of-decline images. The decreasing rate of DAT density in the caudate nucleus was the fastest within the striatum. The finding suggests that neuronal cell loss in the substantia nigra may be associated with age-related DAT decline in the striatum. The consistent association of the regional change in the decreasing rate between DATs and D_2Rs clearly demonstrated that the age-related DAT decline is associated functionally with the age-related D_2R decline. For investigating detailed regional mechanisms, the age-related slope-of-decline images were very useful.

ACKNOWLEDGMENTS

The authors thank Kazunori Kawamura, PhD; Takashi Oda, PhD; Miyoko Ando, RN; and Hiroko Tsukinari, RN, for their technical assistance.

REFERENCES

Allard P, Marcusson JO. 1989. Age-correlated loss of dopamine uptake sites labeled with [^{3}H]GBR-12935 in human putamen. Neurobiol Aging 10:661–664.

Antonini A, Leenders KL, Reist H, Thomann R, Beer HF, Locher J. 1993. Effect of age on D2 dopamine receptors in normal human brain measured by positron emission tomography and 11C-raclopride. Arch Neurol 50:474–480.

Bannon MJ, Whitty CJ. 1997. Age-related and regional differences in dopamine transporter mRNA expression in human midbrain. Neurology 48:969–977.

De Keyser J, Ebinger G, Vauquelin G. 1990. Age-related changes in the human nigrostriatal dopaminergic system. Ann Neurol 27:157–161.

Fearnley JM, Lees AJ. 1991. Ageing and Parkinson's disease: Substantia nigra regional selectivity. Brain 114 (Part 5):2283–2301.

Frost JJ, Rosier AJ, Reich SG, Smith JS, Ehlers MD, Snyder SH, Ravert HT, Dannals RF. 1993. Positron emission tomographic imaging of the dopamine transporter with 11C-WIN 35,428 reveals marked declines in mild Parkinson's disease. Ann Neurol 34:423–431.

Fujiwara T, Watanuki S, Yamamoto S, Miyake M, Seo S, Itoh M, Ishii K, Orihara H, Fukuda H, Satoh T, Kitamura K, Tanaka K, Takahashi S. 1997. Performance evaluation of a large axial field-of-view PET scanner: SET-2400W. Ann Nucl Med 11:307–313.

Giardino L. 1996. Right-left asymmetry of D1- and D2-receptor density is lost in the basal gangha of old rats. Brain Res 720:235–238.

Gibb WR, Lees AJ. 1991. Anatomy, pigmentation, ventral and dorsal subpopulations of the substantia nigra, and differential cell death in Parkinson's disease. J Neurol Neurosurg Psychiatry 54:388–396.

Giros B, Sokoloff P, Martres MP, Riou JF, Emorine LJ, Schwartz JC. 1989. Alternative splicing directs the expression of two D2 dopamine receptor isoforms. Nature 342:923–926.

Gispert JD, Pascau J, Reig S, Martinez-Lazaro R, Molina V, Garcia-Barreno P, Desco M. 2003. Influence of the normalization template on the outcome of statistical parametric mapping of PET scans. Neuroimage 19:601–612.

Guivarc'h D, Vernier P, Vincent JD. 1995. Sex steroid hormones change the differential distribution of the isoforms of the D2 dopamine receptor messenger RNA in the rat brain. Neuroscience 69:159–166.

Gunn RN, Lammertsma AA, Hume SP, Cunningham VJ. 1997. Parametric imaging of ligand-receptor binding in PET using a simplified reference region model. Neuroimage 6:279–287.

Han Z, Kuyatt BL, Kochman KA, DeSouza EB, Roth GS. 1989. Effect of aging on concentrations of D2-receptor-containing neurons in the rat striatum. Brain Res 498:299–307.

Ishikawa T, Dhawan V, Kazumata K, Chaly T, Mandel F, Neumeyer J, Margouleff C, Babchyck B, Zanzi I, Eidelberg D. 1996. Comparative nigrostriatal dopaminergic imaging with iodine-123-beta CIT-FP/SPECT and fluorine-18-FDOPA/PET. J Nucl Med 37:1760–1765.

Kawamura K, Oda K, Ishiwata K. 2003. Age-related changes of the [^{11}C]CFT binding to the striatal dopamine transporters in the Fischer 344 rats: a PET study. Ann Nucl Med 17:249–253.

Kazumata K, Dhawan V, Chaly T, Antonini A, Margouleff C, Belakhlef A, Neumeyer J, Eidelberg D. 1998. Dopamine transporter imaging with fluorine-18-FPCIT and PET. J Nucl Med 39:1521–1530.

L'Hirondel M, Cheramy A, Godeheu G, Artaud F, Saiardi A, Borrelli E, Glowinski J. 1998. Lack of autoreceptor-mediated inhibitory control of dopamine release in striatal synaptosomes of D2 receptor-deficient mice. Brain Res 792:253–262.

Laakso A, Vilkman H, Alakare B, Haaparanta M, Bergman J, Solin O, Peurasaari J, Rakkolainen V, Syvalahti E, Hietala J. 2000. Striatal dopamine transporter binding in neuroleptic-naive patients with schizophrenia studied with positron emission tomography. Am J Psychiatry 157:269–271.

Langer ONK, Dolle F, Lundkvist C, Sandell J, Swahn CG, Vaufrey F, Crouzel C, Maziere B, Halldin C. 1999. Precursor synthesis and radiolabelling of the dopamine D2 receptor ligand [^{11}C]raclopride from [^{11}C]methyl triflate. J Labelled Comp Radiopharm 42:1183–1193.

Larisch R, Meyer W, Klimke A, Kehren F, Vosberg H, Muller-Gartner HW. 1998. Left-right asymmetry of striatal dopamine D2 receptors. Nucl Med Commun 19:781–787.

Meng SZ, Ozawa Y, Itoh M, Takashima S. 1999. Developmental and age-related changes of dopamine transporter, and dopamine D1 and D2 receptors in human basal ganglia. Brain Res 843:136–144.

Mercuri NB, Saiardi A, Bonci A, Picetti R, Calabresi P, Bernardi G, Borrelli E. 1997. Loss of autoreceptor function in dopaminergic neurons from dopamine D2 receptor deficient mice. Neuroscience 79:323–327.

Meyer JH, Gunn RN, Myers R, Grasby PM. 1999. Assessment of spatial normalization of PET ligand images using ligand-specific templates. Neuroimage 9:545–553.

Monsma FJ Jr, McVittie LD, Gerfen CR, Mahan LC, Sibley DR. 1989. Multiple D2 dopamine receptors produced by alternative RNA splicing. Nature 342:926–929.

Piccini P, Whone A. 2004. Functional brain imaging in the differential diagnosis of Parkinson's disease. Lancet Neurol 3:284–290.

Picetti R, Saiardi A, Abdel Samad T, Bozzi Y, Baik JH, Borrelli E. 1997. Dopamine D2 receptors in signal transduction and behavior. Crit Rev Neurobiol 11:121–142.

Pirker W, Asenbaum S, Hauk M, Kandlhofer S, Tauscher J, Willeit M, Neumeister A, Praschak-Rieder N, Angelberger P, Brucke T. 2000. Imaging serotonin and dopamine transporters with 123I-beta-CIT SPECT: binding kinetics and effects of normal aging. J Nucl Med 41:36–44.

Pohjalainen T, Rinne JO, Nagren K, Syvalahti E, Hietala J. 1998. Sex differences in the striatal dopamine D2 receptor binding characteristics in vivo. Am J Psychiatry 155:768–773.

Reeves S, Bench C, Howard R. 2002. Ageing and the nigrostriatal dopaminergic system. Int J Geriatr Psychiatry 17:359–370.

Reig S, Penedo M, Gispert JD, Pascau J, Sanchez-Gonzalez J, Garcia-Barreno P, Desco M. 2007. Impact of ventricular enlargement on the measurement of metabolic activity in spatially normalized PET. Neuroimage 35:748–758.

Rinne JO. 1987. Muscarinic and dopaminergic receptors in the aging human brain. Brain Res 404:162–168.

Rinne JO, Hietala J, Ruotsalainen U, Sako E, Laihinen A, Nagren K, Lehikoinen P, Oikonen V, Syvalahti E. 1993. Decrease in human striatal dopamine D2 receptor density with age: A PET study with [^{11}C]raclopride. J Cereb Blood Flow Metab 13:310–314.

Rinne JO, Lonnberg P, Marjamaki P. 1990. Age-dependent decline in human brain dopamine D1 and D2 receptors. Brain Res 508:349–352.

Rinne JO, Sahlberg N, Ruottinen H, Nagren K, Lehikoinen P. 1998. Striatal uptake of the dopamine reuptake ligand [^{11}C]beta-CFT is reduced in Alzheimer's disease assessed by positron emission tomography. Neurology 50:152–156.

Sakata M, Farooqui SM, Prasad C. 1992. Post-transcriptional regulation of loss of rat striatal D2 dopamine receptor during aging. Brain Res 575:309–314.

Seeman P, Bzowej NH, Guan HC, Bergeron C, Becker LE, Reynolds GP, Bird ED, Riederer P, Jellinger K, Watanabe S, Tourtellotte WW. 1987. Human brain dopamine receptors in children and aging adults. Synapse 1:399–404.

Severson JA, Marcusson J, Winblad B, Finch CE. 1982. Age-correlated loss of dopaminergic binding sites in human basal ganglia. J Neurochem 39:1623–1631.

Stanford JA, Hebert MA, Gerhardt GA. 2001. Biochemical and anatomical changes in basal ganglia of aging animals.Hof PR, Mobbs cV, editors. San Diego: Academic Press. 727–736 p.

Stark AK, Pakkenberg B. 2004. Histological changes of the dopaminergic nigrostriatal system in aging. Cell Tissue Res 318:81–92.

Szabo J. 1980. Organization of the ascending striatal afferents in monkeys. J Comp Neurol 189:307–321.

Thobois S, Jahanshahi M, Pinto S, Frackowiak R, Limousin-Dowsey P. 2004. PET and SPECT functional imaging studies in Parkinsonian syndromes: From the lesion to its consequences. Neuroimage 23:1–16.

Toga AW, Thompson PM. 2003. Mapping brain asymmetry. Nat Rev Neurosci 4:37–48.

van Dyck CH, Seibyl JP, Malison RT, Laruelle M, Wallace E, Zoghbi SS, Zea-Ponce Y, Baldwin RM, Charney DS, Hoffer PB. 1995. Age-related decline in striatal dopamine transporter binding with iodine-123-beta-CITSPECT. J Nucl Med 36:1175–1181.

Vernaleken I, Weibrich C, Siessmeier T, Buchholz HG, Rosch F, Heinz A, Cumming P, Stoeter P, Bartenstein P, Grunder G. 2007. Asymmetry in dopamine D(2/3) receptors of caudate nucleus is lost with age. Neuroimage 34:870–878.

Volkow ND, Fowler JS, Wang GJ, Logan J, Schlyer D, MacGregor R, Hitzemann R, Wolf AP. 1994. Decreased dopamine transporters with age in health human subjects. Ann Neurol 36:237–239.

Volkow ND, Ding YS, Fowler JS, Wang GJ, Logan J, Gatley SJ. Hitzemann R, Smith G, Fields SD, Gur R. 1996a. Dopamine transporters decrease with age. J Nucl Med 37:554–559.

Volkow ND, Wang GJ, Fowler JS, Logan J, Gatley SJ, MacGregor RR, Schlyer DJ, Hitzemann R, Wolf AP. 1996b. Measuring age-related changes in dopamine D2 receptors with 11C-raclopride and 18F-N-methylspiroperidol. Psychiatry Res 67:11–16.

Volkow ND, Wang GJ, Fowler JS, Ding YS, Gur RC, Gatley J, Logan J, Moberg PJ, Hitzemann R, Smith G, Pappas N. 1998. Parallel loss of presynaptic and postsynaptic dopamine markers in normal aging. Ann Neurol 44:143–147.

Wong DF, Broussolle EP, Wand G, Villemagne V, Dannals RF, Links JM, Zacur HA, Harris J, Naidu S, Braestrup C, Wagner HN Jr, Gjedde A. 1988. In vivo measurement of dopamine receptors in human brain by positron emission tomography. Age and sex differences. Ann NY Acad Sci 515:203–214.

Wong DF, Yung B, Dannals RF, Shaya EK, Ravert HT, Chen CA, Chan B, Folio T, Scheffel U, Ricaurte GA, Neumeyer JL, Wagner HN Jr, Kuhar MJ. 1993. In vivo imaging of baboon and human dopamine transporters by positron emission tomography using [^{11}C]WIN 35,428. Synapse 15:130–142.

Wong DF, Young D, Wilson PD, Meltzer CC, Gjedde A. 1997. Quantification of neuroreceptors in the living human brain. III. D2-like dopamine receptors: Theory, validation, and changes during normal aging. J Cereb Blood Flow Metab 17:316–330.

Zelnik N, Angel I, Paul SM, Kleinman JE. 1986. Decreased density of human striatal dopamine uptake sites with age. Eur J Pharmacol 126:175–176.

Ann Nucl Med (2008) 22:841–847
DOI 10.1007/s12149-008-0185-5

ORIGINAL ARTICLE

Adenosine A_1 receptors using 8-dicyclopropylmethyl-1-[^{11}C]methyl-3-propylxanthine PET in Alzheimer's disease

**Nobuyoshi Fukumitsu · Kenji Ishii · Yuichi Kimura
Keiichi Oda · Masaya Hashimoto · Masahiko Suzuki
Kiichi Ishiwata**

Received: 5 September 2007 / Accepted: 19 June 2008

Abstract
Objective Adenosine is an endogenous modulator of synaptic functions in the central nervous system. The effects of adenosine are mediated by at least four adenosine receptor subtypes. Decreased density of adenosine A_1 receptors, which is a major subtype adenosine receptor in the hippocampus, has been reported in vitro in Alzheimer's disease. We evaluated adenosine A_1 receptor in the brain of elderly normal subjects and patients with Alzheimer's disease (n = 8 and 6, respectively), using positron emission tomography (PET) and 8-dicyclopropylmethyl-1-[^{11}C]methyl-3-propylxanthine ([^{11}C]MPDX).
Methods A 60-min PET scan with [^{11}C]MPDX was performed. The patients with Alzheimer's disease also underwent PET with [^{18}F]fluorodeoxyglucose (FDG). The binding potential of [^{11}C]MPDX was quantitatively calculated in the regions of interest (ROIs) placed on the frontal, medial frontal, temporal, medial temporal, parietal, and occipital cortices, striatum, thalamus, cerebellum, and pons. Statistical parametric mapping (SPM2) was used for analysis of [^{11}C]MPDX and FDG-PET.
Results In the ROI-based analysis, the binding potential of [^{11}C]MPDX in patients with Alzheimer's disease was significantly lower in the temporal and medial temporal cortices and thalamus than that in elderly normal subjects (P = 0.038, 0.028, and 0.039, respectively). SPM analysis also showed significant decreased binding potential in the temporal and medial temporal cortices and thalamus in patients with Alzheimer's disease. FDG uptake was significantly decreased in the temporoparietal cortex and posterior cingulate gyrus.
Conclusions Decreased binding of [^{11}C]MPDX in patients with Alzheimer's disease was detected in temporal and medial temporal cortices and thalamus. This pattern possibly differed from the hypometabolism pattern of FDG. [^{11}C]MPDX PET is valuable for the detection of degeneration in the temporal and medial temporal cortices and corticothalamic transmission, and may provide a different diagnostic tool from FDG-PET in brain disorders such as Alzheimer's disease.

Keywords [^{11}C]MPDX · Adenosine A_1 receptor · Medial temporal cortex · Positron emission tomography · Alzheimer's disease

N. Fukumitsu (✉)
2-1-1-204 Midoridai, Funabashi, Chiba 274-0818, Japan
e-mail: fukumitsun@yahoo.co.jp

N. Fukumitsu
Proton Medical Research Center, University of Tsukuba, Ibaraki, Japan

N. Fukumitsu · K. Ishii · Y. Kimura · K. Oda · K. Ishiwata
Positron Medical Center, Tokyo Metropolitan Institute of Gerontology, Tokyo, Japan

M. Hashimoto · M. Suzuki
Department of Neurology, Jikei University School of Medicine, Tokyo, Japan

Introduction

Adenosine is present in large amounts in the mammalian brain and plays a role as an endogenous modulator of synaptic functions in the central nervous system. Prior work has established a role for adenosine in a diverse array of neural phenomena, which include regulation of

sleep and the level of arousal, neuroprotection, regulation of seizure susceptibility, locomotor effects, analgesia, mediation of the effects of ethanol, and chronic drug use [1]. Therefore, interaction with the adenosine metabolism is a promising target for therapeutic intervention in ischemic, neurological, and psychiatric disorders [2–4].

The effects of adenosine are mediated by at least four adenosine receptor subtypes, namely, A_1, A_{2A}, A_{2B}, and A_3. The two major subtypes of receptors, namely, A_1 and A_2 receptors, have been well investigated in molecular biology, pharmacology, and physiology [4–6]. Adenosine presynaptically inhibits the release of many neurotransmitters, especially excitatory ones such as the potentially excitotoxic amino acid glutamate [7, 8]. This effect of adenosine is mediated by presynaptic A_1 receptors linked via G-proteins to both calcium and potassium ion channels [9–12].

Alzheimer's disease is the most common form of age-related dementia and one of the most serious health problems. Dementia affects approximately 1–5% of the population more than 65 years of age [13] and 20–40% of the population more than 80 years of age [14, 15]. The economic and social burdens of Alzheimer's disease on families have been documented in many studies [16–18]. In studies on the postmortem brain with Alzheimer's disease, decreased density of adenosine A_1 receptor in the hippocampus has been reported [19–22]. Ulas et al. [20] reported that the reduction in the adenosine A_1-specific ligand-receptor binding was owing to a decrease in the density of binding sites (B_{max}), but was not owing to changes in the affinity (K_d) [20]. With regard to the clinical diagnosis of Alzheimer's disease, positron emission tomography (PET) using [^{18}F]fluorodeoxyglucose (FDG) is the most popular method, and reduction of glucose metabolism is prominent in the temporo-parietal cortex and posterior cingulate gyrus. However, hypometabolism in the medial temporal cortex has not necessarily been detected as a symptom of Alzheimer's disease, although morphological changes are prominent in the medial temporal cortex [23–25].

Recently, we successfully performed imaging of adenosine A_1 receptors in the human brain of normal young volunteers using PET with 8-dicyclopropylmethyl-1-[^{11}C]methyl-3-propylxanthine ([^{11}C]MPDX) [26–29]. In the present study, we investigated the change of the adenosine A_1 receptors in patients with Alzheimer's disease with [^{11}C]MPDX PET. We also examined the same patients with FDG-PET for direct comparison of the two diagnostic tools. This report is a preliminary study of the utility of [^{11}C]MPDX PET in the diagnosis of patients with Alzheimer's disease.

Materials and methods

The study protocol was approved by the Institutional Ethical Committee. Eight normal elderly volunteers [men 66.9 ± 6.5 (61–75) years] were enrolled together with six Alzheimer's disease patients [men, $n = 5$; women, $n = 1$; 73.5 ± 9.8 (58–83) years]. A written informed consent was obtained from all the participants in this study. It was confirmed that no participants received xanthine-type drugs such as theophylline for asthma.

All the normal subjects were healthy according to the history, physical, neurological and psychiatric examinations, and a magnetic resonance imaging (MRI) study of the brain prior to the PET study. In the psychiatric examination, we used the Hospital Anxiety and Depression Scale [30].

All the patients with Alzheimer's disease showed mild-to-moderate dementia and were diagnosed according to the National Institute of Neurological and Communicative Diseases and Stroke/Alzheimer's Disease and Related Disorders Association (NINCDS–ADRDA) criteria. The disease duration following the first onset of memory disturbance was 0–4 years. We performed clinical assessments, including neuropsychological testing and exclusion of other diseases, with computed tomography or MRI as required by the NINCDS–ADRDA criteria. The exclusion criteria were prior episodes of subarachnoid or intracerebral hemorrhage, intracranial tumors, hydrocephalus, all psychoses (including major depression), alcoholism, epilepsy, ischemic strokes, vascular dementia, sleep disorders, and other forms of dementia, anemia, and nonstabilized diabetes mellitus. The patients who were suspected to have other diseases with neurodegeneration from the FDG-PET findings or who were on medications that affect the brain circulation or metabolism were excluded, and especially acethylcholinesterase blockers were not given prior to the PET study. The Mini-Mental State Examination score was 20–24. Neither normal subjects nor patients with Alzheimer's disease complained about their sleep behavior.

PET measurement

Radiosynthesis of [^{11}C]MPDX was performed as described earlier [31, 32]. PET measurement was performed with an SET-2400W system (Shimadzu, Kyoto, Japan), which acquires 63 slices having 128 × 128 pixels each at a transverse resolution of 4.5 mm full width at half maximum (FWHM) and at an axial resolution of 5.8 mm FWHM. Scanning took place as the subjects lay supine. A venous catheter was inserted into the forearm vein of the subjects for tracer injection, and an arterial

catheter was inserted into the distal radial artery under local anesthesia for arterial blood sampling. After positioning the subject's head in the canthomeatal orientation and fixing the subject's head using a band to prevent movement during the examination, a transmission scan was performed with a rotating [^{68}Ga]/[^{68}Ge] line source to correct for the photon attenuation using the attenuation map. All the subjects were given [^{11}C]MPDX [611 ± 123 (300–757) MBq/14.4 ± 12.5 (2.8–47.5 nmol)] for a period of 10 s, and the PET scan and arterial blood sampling were performed for 60 min as described earlier [27]. We did not impose any meal restriction for [^{11}C]MPDX PET.

In all patients with Alzheimer's disease, FDG-PET was also done on the same day or within 3 months. The subjects each received an intravenous injection of FDG [128 ± 13 (107–142) MBq]. Starting 45 min post-injection, an emission scan was performed for 6 min following a transmission scan using ^{68}Ge for attenuation correction. In the case of one of the six patients who underwent both [^{11}C]MPDX PET and FDG-PET on the same day, the former was carried out in the morning, with FDG administered 3 h later.

Kinetic analysis

The PET images were registered and resliced to the MRI with Ardekani's-image registration algorithm [33] using UNIX workstations (Silicon Graphics, Mountain View, CA, USA) with the Dr. View image analysis software system (AJS, Tokyo, Japan). Regions of interest (ROIs) were placed on the frontal, medial frontal, temporal, medial temporal, parietal, and occipital cortices, striatum, thalamus, cerebellum, and pons based on MRI (Fig. 1). The ROI on the frontal cortex had 1582 ± 275 voxels and that on the pons had 85 ± 3 voxels (1 voxel = 2 mm × 2 mm × 6.25 mm). The voxel numbers on other regions were in-between these values. Using the time–activity curves for each ROI of the brain and the metabolite-corrected time–activity curve of plasma, the distribution volume (DV) of [^{11}C]MPDX in each ROI was calculated by graphical analysis using Logan plots according to the method as described earlier [27, 28]. The binding potential in each ROI was then obtained as follows [28]:

$$\text{Binding potential} = DV_{(\text{region})}/DV_{(\text{cerebellum})} - 1.$$

The binding potential in each ROI was expressed as mean values ± standard deviations. The difference of the binding potential in each ROI was respectively tested between normal elderly subjects group and patients with Alzheimer's disease group using Mann–Whitney U test.

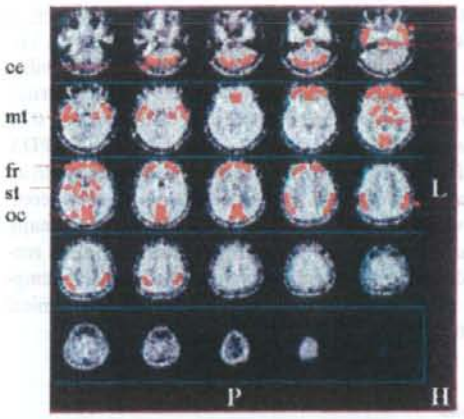

Fig. 1 Region of interest mapping of 8-dicyclopropylmethyl-1-[^{11}C]methyl-3-propylxanthine positron emission tomography ([^{11}C]MPDX PET). *fr* frontal cortex, *mf* medial frontal cortex, *te* temporal cortex, *mt* medial temporal cortex, *pa* parietal cortex, *oc* occipital cortex, *st* striatum, *th* thalamus, *ce* cerebellum, *po* pons

Statistical significance was assumed at $P < 0.05$. In FDG-PET, regional glucose metabolism was expressed using standardized uptake value (SUV).

Statistical parametric mapping analysis

The PET images were analyzed using SPM2 software (Wellcome Department of Cognitive Neurology, Institute of Neurology, London, UK), implemented using Matlab 7.0 (MathWorks, Sherborn, MA, USA). For this purpose, binding potential image of [^{11}C]MPDX and SUV image of FDG were used. Prior to statistical analysis, all the images were spatially normalized into the MNI standard space (Montreal Neurological Institute, McGill University, Montreal, QC, Canada) using house-made templates for [^{11}C]MPDX and FDG-PET images, to remove inter-subject anatomical variability. In normalization of [^{11}C]MPDX PET, total DV image that well reflected brain anatomical structure including cerebellum was used. Spatially normalized images were smoothed by convolution, using an isotropic Gaussian kernel with 16 mm FWHM. The aim of smoothing was to increase the signal-to-noise ratio and to account for the subtle variations in anatomical structures. The count of each voxel in FDG-PET was normalized to the global mean (value = 50) with proportional scaling in SPM2. No global normalization was applied to the [^{11}C]MPDX PET because binding potential was quantitatively calculated. After spatial and count normalization, statistical comparisons between groups were performed on a voxel-by-voxel basis using t statistics, generating SPM (t)

maps. In FDG-PET, the data of the normal elderly template in our institute ($n = 41$, 51–78 years) were used as a reference for the patients with Alzheimer's disease. The data of the normal volunteers whose age and eligibility were matched with this protocol were used in normal elderly template. Thresholds of $P < 0.005$ and $P < 0.01$ corrected for the cluster level were applied to [^{11}C]MPDX and FDG-PET images, respectively. The clusters with an extent of greater than 300 voxels were considered. For visualization of the t score statistics [SPM (t) map], the significant voxels were projected onto the 3D rendered brain of a standard high-resolution MRI template provided by SPM2, thus allowing anatomical identification.

Results

In the ROI-based analysis, the binding potential of [^{11}C]MPDX in normal elderly subjects was high in the striatum and thalamus and low in the cerebellum and pons. The binding potential of [^{11}C]MPDX in patients with Alzheimer's disease was high in the striatum and thalamus and low in the medial temporal cortex and cerebellum. The binding potential of [^{11}C]MPDX in patients with Alzheimer's disease was significantly lower in the temporal, medial temporal cortices, and thalamus than that in normal elderly subjects ($P = 0.038$, 0.028, and 0.039, respectively; Fig. 2). Especially, the binding potential of [^{11}C]MPDX in the medial temporal cortex in patients with Alzheimer's disease was nearly equal to that in the cerebellum.

The SPM analysis of [^{11}C]MPDX PET between patients with Alzheimer's disease and normal elderly subjects is shown in Fig. 3a. The binding potential was widely and severely decreased in the temporal, medial temporal cortices, and thalamus, and partially decreased in the parietal cortex in patients with Alzheimer's disease with significance ($P < 0.005$, corrected $k > 300$). Decreased binding potential was slightly prominent in the left hemisphere.

The SPM analysis of FDG-PET in the same patients with Alzheimer's disease is shown in Fig. 3b. The FDG uptake was widely and severely decreased in the temporoparietal cortex and posterior cingulate gyrus with significance ($P < 0.01$, corrected $k > 300$). Decreased FDG uptake was slightly prominent in the left hemisphere.

Discussion

In Alzheimer's disease subjects, ROI-based analysis and SPM analysis clearly demonstrated the decreased binding potential of [^{11}C]MPDX in the temporal and medial temporal cortices and thalamus when compared with normal elderly subjects as shown in Figs. 2 and 3a. The finding of decreased binding potential in the medial temporal cortex is consistent with past postmortem autoradiographic and pathological studies of patients with Alzheimer's disease [19–22]. Ulas et al. [20] reported that decreased A_1 agonist binding was observed in the CA1 stratum oriens and outer layers of the parahippocampal gyrus, whereas decreased antagonist binding was found in the subiculum and CA3 region. Adenosine A_1 recep-

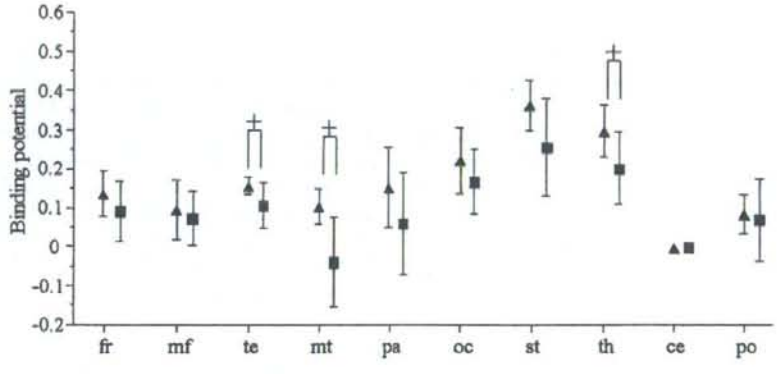

Fig. 2 Binding potential of [^{11}C]MPDX in the human brain. Patients with Alzheimer's disease showed a significantly lower value in the temporal and medial temporal cortices and thalamus than normal elderly volunteers. The value in the cerebellum was zero because the value was calculated based on the assumption that adenosine A_1 receptors are very sparse in the cerebellum. Abbreviations used are the same as in Fig. 1. *Triangle* normal elderly subjects ($n = 8$), *square* patients with Alzheimer's disease ($n = 6$), *plus* $P < 0.05$ compared between normal elderly subjects and patients with Alzheimer's disease

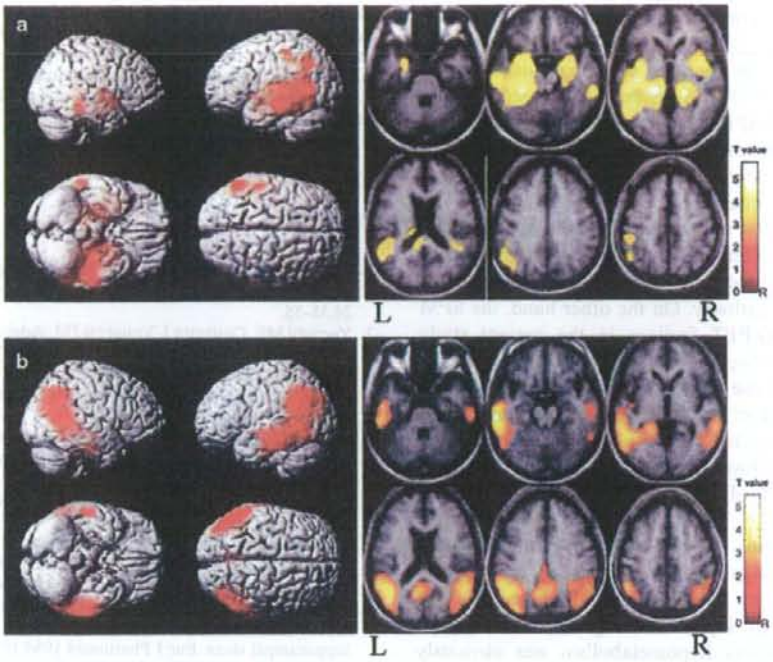

Fig. 3 Statistical analyses of the binding potential of [^{11}C]MPDX (**a**) and standardized uptake value (SUV) of [^{18}F]fluorodeoxyglucose (FDG, **b**) in patients with Alzheimer's disease. *Left* Statistical parametric mapping (SPM) *Z* maps are superimposed onto the right lateral, left lateral, inferior, and superior views (from *left upper* to *right lower*) of a volume-rendered spatially normalized magnetic resonance imaging (MRI) study. *Right* SPM *Z* maps are superimposed onto the axial views of a spatially normalized T1-MRI study. Each image represents from the *bottom* (*left upper*) to the *top* (*right lower*). *Red* and *yellow* represent the areas with significant reduction in binding potential or SUV. **a** Decreased binding potential of [^{11}C]MPDX was noted in the temporal, medial temporal cortices, and thalamus widely and parietal cortex partially. Decreased binding is slightly prominent in the left hemisphere. **b** Decreased SUV of FDG was noted in the temporo-parietal cortices. Decreased SUV is slightly prominent in the left hemisphere

tors are located on the terminal of the perforant pathway which provides a major input to the molecular layer of the dentate gyrus [34]. It has been reported that the perforant pathway contributes 80%–85% of the synapses on the outer portion of the dendrites that arise from the dentate gyrus granule cells [34, 35]. The cells of origin of the perforant pathway in the entorhinal cortex are destroyed in the brain of patients with Alzheimer's disease [34]. Decreased binding potential of [^{11}C]MPDX in the medial temporal cortex is considered to be affected by insufficiency or damage to the perforant pathway in patients with Alzheimer's disease. Decreased binding potential of [^{11}C]MPDX in the temporal cortex in patients with Alzheimer's disease can be directly or indirectly correlated with destruction of the cells of origin of the perforant pathway. Thalamic nuclei have strong reciprocal connections with the cerebral cortex, forming thalamo-cortico-thalamic circuits. An abnormal finding in the thalamus of Alzheimer's disease has been described in a few MRI reports [36, 37]. It is considered that decreased binding potential of [^{11}C]MPDX in the thalamus is derived from corticothalamic transmission from the temporal and medial temporal cortices. The reason for the laterality in [^{11}C]MPDX and FDG-PET can be derived from investigations of small numbers ($n = 6$) of patients. Laterality in FDG-PET was also reported in a study with a small number of patients with Alzheimer's disease [38]. It is necessary to investigate these issues in greater number of patients.

We calculated the binding potential as a reference for the cerebellar cortex because the cerebellar cortex showed very low adenosine A_1 receptor densities [39] and this method provided well-balanced data in our earlier study [28]. The calculated binding potential of [^{11}C]MPDX in the medial temporal cortex was slightly lower than 0, which means that adenosine A_1 receptor density in the

medial temporal cortex in patients with Alzheimer's disease is nearly equal to or lower than that in the cerebellar cortex which contains very low adenosine A_1 receptor densities [39]. A severely decreased binding potential of [^{11}C]MPDX in the medial temporal cortex means that the perforant pathway in the medial temporal cortex is markedly insufficient or damaged in patients with Alzheimer's disease.

We consider that the decreased binding potential of [^{11}C]MPDX in the temporal and medial temporal cortices directly or indirectly reflects insufficiency or damage to the perforant pathway. On the other hand, the SPM analysis of FDG-PET findings in the present study revealed that FDG uptake was decreased in the temporal cortex and not in the medial temporal cortex, where the binding potential of [^{11}C]MPDX decreased markedly. The findings suggested that insufficiency or damage to the perforant pathway in the medial temporal cortex could not necessarily be reflected by the FDG-PET results.

Hypometabolism in the temporo-parietal cortex and posterior cingulate gyrus (Fig. 3b) is a typical pattern revealed by FDG-PET in Alzheimer's disease subjects [23–25, 40, 41]. In the temporo-parietal cortex, the area with severe hypometabolism was obviously larger than that with decreased binding potential of [^{11}C]MPDX in patients with Alzheimer's disease. In the posterior cingulate gyrus, [^{11}C]MPDX PET was not coupled with hypometabolism. Therefore, FDG-PET is more sensitive in detecting the degeneration of the temporo-parietal cortex and posterior cingulate gyrus, which is a typical manifestation in Alzheimer's disease, than [^{11}C]MPDX PET. However, it is well known that FDG-PET in Alzheimer's disease does not necessary reflect the pathological changes [42–44]. [^{11}C]MPDX PET provides a different diagnostic tool than FDG-PET, and could be valuable in detecting the degeneration in the medial temporal cortex. In addition, [^{11}C]MPDX PET has the possibility to detect corticothalamic transmission from the temporal and medial temporal cortices.

Conclusions

In patients with Alzheimer's disease, the binding potential of [^{11}C]MPDX decreased significantly in the temporal and medial temporal cortices and thalamus, and a small or no decrease was observed in the parietal cortex and posterior cingulate gyrus. The pattern of the binding potential of [^{11}C]MPDX had the possibility to be different from that of the FDG-PET in patients with Alzheimer's disease.

Acknowledgments This work was supported by Grants-in-Aid for Scientific Research (B) Nos. 16390348 and 20390334 from the Japan Society for the Promotion of Science. The authors thank Dr. Kazunori Kawamura for the preparation of [^{11}C]MPDX and Ms. Miyoko Ando for her care of the subjects during the PET measurement.

References

1. Dunwiddie TV, Masino SA. The role and regulation of adenosine in the central nervous system. Ann Rev Neurosci 2001; 24:31–55.
2. Yacoubi ME, Costentin J, Vaugeois JM. Adenosine A_{2A} receptors and depression. Neurology 2003;61:S82–7.
3. von Lubitz DK. Adenosine in the treatment of stroke: yes, maybe, or absolutely not? Expert Opin Investig Drugs 2001; 10:619–32.
4. Haas HL, Selbach O. Functions of neuronal adenosine receptors. Naunyn Schmiedebergs Arch Pharmacol 2000;362: 375–81.
5. Collis MG, Hourani SMO. Adenosine receptor subtypes. Trends Pharmacol Sci 1993;14:360–6.
6. Fredholm BB, Abbracchio MP, Burnstock G, Daly JW, Harden TK, Jacobson KA, et al. Nomenclature and classification of purinoceptors. Pharmacol Rev 1994;46:143–56.
7. Corradetti R, Lo Conte G, Moroni F, Passani MB, Pepeu G. Adenosine decreases aspartate and glutamate release from rat hippocampal slices. Eur J Pharmacol 1984;104:19–26.
8. Dolphin AC, Archer ER. An adenosine agonist inhibits and a cyclic AMP analogue enhances the release of glutamate but not GABA from slices of rat dentate gyrus. Neurosci Lett 1983;43:49–54.
9. Dunwiddie TV. The physiological role of adenosine in the central nervous system. Int Rev Neurobiol 1985;27:63–139.
10. Fredholm BB, Dunwiddie TV. How does adenosine inhibit transmitter release? Trends Pharmacol Sci 1988;9:130–4.
11. Fredholm BB, Hedqvist P. Modulation of neurotransmission by purine nucleotides and nucleosides. Biochem Pharmacol 1980;29:1635–43.
12. Phillis JW, Wu PH. The role of adenosine and its nucleotides in central synaptic transmission. Prog Neurobiol 1981;16: 187–239.
13. Schoenberg BS. Epidemiology of Alzheimer's disease and other dementing disorders. J Chronic Dis 1986;39:1095–104.
14. Fratiglioni L, Grut M, Forsell Y, Viitanen M, Grafstrom M, Holmen K, et al. Prevalence of Alzheimer's disease and other dementias in an elderly urban population: relationship with age, sex, and education. Neurology 1991;41:1886–92.
15. Brookmeyer R, Gray S, Kawas C. Projections of Alzheimer's disease in the United States and the public health impact of delaying disease onset. Am J Public Health 1998;88:1337–42.
16. Weinberger M, Gold DT, Divine GW, Cowper PA, Hodgson LG, Schreiner PJ, et al. Expenditures in caring for patients with dementia who live at home. Am J Public Health 1993; 83:338–41.
17. Osttbye T, Crosse E. Net economic costs of dementia in Canada. CMAJ 1994;151:1457–63.
18. Ernst R, Hay JW, Fenn C, Tinklenberg J, Yesavage JA. Cognitive function and the costs of Alzheimer's disease. Arch Neurol 1997;54:687–93.
19. Jansen K, Faull RLM, Dragunow M, Synek BJL. Alzheimer's disease: changes in hippocampal *N*-methyl-D-aspartate, quisqualate, neurotensin, adenosine, benzodiazepine, sero-

tonin and opioid receptors: an autoradiographic study. Neuroscience 1990;39:613–27.
20. Ulas J, Brunner LC, Nguyen L, Cotman CW. Reduced density of adenosine A1 receptors and preserved coupling of adenosine A1 receptors to G proteins in Alzheimer hippocampus: a quantitative autoradiographic study. Neuroscience 1993;52: 843–54.
21. Jaarsma D, Sebens B, Korf J. Reduction of adenosine A1-receptors in the perforant pathway terminal zone in Alzheimer hippocampus. Neurosci Lett 1991;121:111–4.
22. Kalaria RN, Sromek S, Wilcox BJ, Unnerstall JR. Hippocampal adenosine A1 receptors are decreased in Alzheimer's disease. Neurosci Lett 1990;118:257–60.
23. Ishii K, Sasaki H, Kono AK, Miyamoto N, Fukuda T, Mori E. Comparison of gray matter and metabolic reduction in mild Alzheimer's disease using FDG-PET and voxel-based morphometric MR studies. Eur J Nucl Med 2005;32:959–63.
24. Mosconi L. Brain glucose metabolism in the early and specific diagnosis of Alzheimer's disease. FDG-PET studies in MCI and AD. Eur J Nucl Med 2005;32:486–510.
25. Meguro K, LeMestric C, Landeau B, Desgranges B, Eustache F, Baron JC. Relations between hypometabolism in the posterior association neocortex and hippocampal atrophy in Alzheimer's disease: a PET/MRI correlative study. J Neurol Neurosurg Psychiatry 2001;71:315–21.
26. Fukumitsu N, Ishii K, Kimura Y, Oda K, Sasaki T, Mori Y, et al. Imaging of adenosine A_1 receptors in the human brain by positron emission tomography with [^{11}C]MPDX. Ann Nucl Med 2003;17:511–5.
27. Fukumitsu N, Ishii K, Kimura Y, Oda K, Sasaki T, Mori Y, et al. Adenosine A_1 receptor mapping of the human brain by PET with 8-dicyclopropylmethyl-1-11C-methyl-3-propylxanthine. J Nucl Med 2005;46:32–7.
28. Kimura Y, Ishii K, Fukumitsu N, Oda K, Sasaki T, Kawamura K, et al. Quantitative analysis of adenosine A_1 receptors in human brain using positron emission tomography and [1-methyl-^{11}C]8-dicyclopropylmethyl-1-methyl-3-propylxanthine. Nucl Med Biol 2004;31:975–81.
29. Naganawa M, Kimura Y, Nariai T, Ishii K, Oda K, Manabe Y, et al. Omission of serial arterial blood sampling in neuroreceptor imaging with independent component analysis. Neuroimage 2005;26:885–90.
30. Zigmond AS, Snaith RP. The Hospital Anxiety and Depression Scale. Acta Psychiatr Scand 1983;67:361–7.
31. Noguchi J, Ishiwata K, Furuta R, Simada J, Kiyosawa M, Ishii S, et al. Evaluation of carbon-11 labeled KF15372 and its ethyl and methyl derivatives as a potential CNS adenosine A_1 receptor ligand. Nucl Med Biol 1997;24:53–9.
32. Ishiwata K, Nariai T, Kimura Y, Oda K, Kawamura K, Ishii K, et al. Preclinical studies on [^{11}C]MPDX for mapping adenosine A_1 receptors by positron emission tomography. Ann Nucl Med 2002;16:377–82.
33. Ardekani BA, Braun M, Hutton BF, Kanno I, Iida H. A fully automatic multimodality image registration algorithm. J Comput Assist Tomog 1995;19:615–23.
34. Dragunow M, Murphy K, Leslie RA, Robertson HA. Localization of adenosine A1-receptors to the terminals of the perforant path. Brain Res 1988;462:252–7.
35. Hyman BT, Van Hoesen GW, Kromer LJ, Damasio AR. Perforant pathway changes and the memory impairment of Alzheimer's disease. Ann Neurol 1986;20:472–81.
36. Stephen RE, Janke AL, Chark JB. Gray and white matter changes in Alzheimer's disease: a diffusion tensor imaging study. J Magn Reson Imaging 2008;27:20–6.
37. Medina D, DeToledo-Morrell L, Urresta F, Gabrieli JD, Moseley M, Fleischman D, et al. White matter changes in mild cognitive impairment and AD: a diffusion tensor imaging study. Neurobiol Aging 2006;27:663–72.
38. Zahn R, Juengling F, Bubrowski P, Jost E, Dykierek P, Talazko J, et al. Hemisphere asymmetries of hypometabolism associated with semantic memory impairment in Alzheimer's disease: a study using positron emission tomography with fluorodeoxygulcose-F18. Psychiatry Res Neuroimaging 2004; 132:159–72.
39. Fastbom J, Pazos A, Probst A, Palacios JM. Adenosine A1 receptors in the human brain: a quantitative autoradiographic study. Neuroscience 1987;22:827–39.
40. Sakamoto S, Ishii K, Sasaki M, Hosaka M, Mori T, Matsui M, et al. Differences in cerebral metabolic impairment between early and late onset types of Alzheimer's disease. J Neurol Sci 2002;15:27–32.
41. Kim EJ, Cho SS, Jeong Y, Park KC, Kang E, Kim SE, et al. Glucose metabolism in early onset versus late onset Alzheimer's disease: an SPM analysis of 120 patients. Brain 2005;128:1790–801.
42. Ibanez V, Pietrini P, Alexander GE, Furey ML, Teichberg D, Rajapakse JC, et al. Regional glucose metabolic abnormalities are not the result of atrophy in Alzheimer's disease. Neurology 1998;50:1585–93.
43. Mosconi L, Sorbi S, de Leon MJ, Li Y, Nacmias B, Myoung PS, et al. Hypometabolism exceeds atrophy in presymptomatic early-onset familial Alzheimer's disease. J Nucl Med 2006;47:1778–86.
44. Chetelat G, Desgranges B, Landeau B, Mezenge F, Poline JB, de la Sayette V, et al. Direct voxel-based comparison between grey matter hypometabolism and atrophy in Alzheimer's disease. Brain 2008;131:60–71.

Ann Nucl Med (2008) 22:151–156
DOI 10.1007/s12149-007-0094-z

ORIGINAL ARTICLE

Low density of sigma$_1$ receptors in early Alzheimer's disease

**Masahiro Mishina · Masashi Ohyama · Kenji Ishii
Shin Kitamura · Yuichi Kimura · Kei-ichi Oda
Kazunori Kawamura · Toru Sasaki · Shiro Kobayashi
Yasuo Katayama · Kiichi Ishiwata**

Received: 24 July 2007 / Accepted: 5 September 2007

Abstract
Objective The sigma$_1$ receptor is considered to be involved in cognitive function. A postmortem study reported that the sigma$_1$ receptors were reduced in the hippocampus in Alzheimer's disease (AD). However, in vivo imaging of sigma$_1$ receptors in the brain of AD patients has not been reported. The aim of this study is to investigate the mapping of sigma$_1$ receptors in AD using [^{11}C]SA4503 positron emission tomography (PET).

Methods We studied five AD patients and seven elderly volunteers. A dynamic series of decay-corrected PET data acquisition was performed for 90 min starting at the time of the injection of 500 MBq of [^{11}C]SA4503. A two-tissue three-compartment model was used to estimate K_1, k_2, k_3, k_4, and the delay between metabolite-corrected plasma and tissue time activity using a Gauss–Newton algorithm. The ratio of k_3 to k_4 was computed as the binding potential (BP), which is linearly related to the density of sigma$_1$ receptors. Unpaired t tests were used to compare K_1 and BP in patients with AD and normal subjects.
Results As compared with normals, BP in the AD was significantly lower in the frontal, temporal, and occipital lobe, cerebellum and thalamus, whereas K_1 was significantly lower in the parietal lobe.
Conclusions [^{11}C]SA4503 PET can demonstrate that the density of cerebral and cerebellar sigma$_1$ receptors is reduced in early AD.

Keywords Alzheimer's disease · Positron emission tomography · Sigma$_1$ receptor · Cortex · Cerebellum

M. Mishina · M. Ohyama · K. Ishii · Y. Kimura · K. Oda · K. Kawamura · T. Sasaki · K. Ishiwata
Positron Medical Center, Tokyo Metropolitan Institute of Gerontology, Tokyo, Japan

M. Mishina · M. Ohyama · S. Kitamura · Y. Katayama
Department of Neurology, Nephrology and Rheumatology, Nippon Medical School, Tokyo, Japan

M. Mishina (✉) · S. Kobayashi
Neurological Institute, Nippon Medical School Chiba-Hokusoh Hospital, 1715 Kamagari, Imba-mura, Imba-gun, Chiba 270-1694, Japan
e-mail: mishina@nms.ac.jp

S. Kitamura
Department of Internal Medicine, Nippon Medical School Musashi Kosugi Hospital, Kanagawa, Japan

Y. Kimura
Biophysics Group, Molecular Imaging Center, National Institute of Radiological Sciences, Chiba, Japan

K. Kawamura
Center for Integrated Brain Science, Brain Research Institute, University of Niigata, Niigata, Japan

T. Sasaki
Research Team for Molecular Biomarkers, Tokyo Metropolitan Institute of Gerontology, Tokyo, Japan

Introduction

Sigma$_1$ receptor has received considerable attention in the regulation of cognitive function [1]. The sigma receptor has been established as a distinct receptor, although it was initially proposed as a subtype of opioid receptors [2]. It is classified into at least two subtypes, namely, sigma$_1$ and sigma$_2$ [3]. Although an endogenous ligand for the sigma receptors remains unclear, some studies have reported that steroid hormones such as progesterone and testosterone might interact with sigma

receptors [4, 5]. Confirmed $sigma_1$ receptor ligand functions are neuro-protective, anti-depressant, and anti-amnestic functions [6, 7]. $Sigma_1$ receptor agonists improved impairment of learning and memory in mice [8–10]. Matsuno et al. [11–13] showed that the $sigma_1$ receptor agonists such as (+)-SKF-10,047 and SA4503 increased extracellular acetylcholine levels in the rat frontal cortex and hippocampus. The $sigma_1$ receptor is considered to be involved in aging [14, 15] and various diseases, such as schizophrenia [16], depression [17], ischemia [18], and Parkinson's disease [19]. In patients with Alzheimer's disease (AD), a postmortem study showed that the $sigma_1$ binding sites were reduced in the hippocampus [20]. The $sigma_1$ receptor agonists are also expected as drugs for improving the cognitive deficits of AD [21]. However, the distribution of $sigma_1$ receptors in patients with AD remains to be determined. We developed a positron emission tomography (PET) ligand, [^{11}C]SA4503 (Fig. 1), for mapping the $sigma_1$ receptors [22–24], and reported that $sigma_1$ receptor was down-regulated in the putamen with Parkinson's disease [19]. The objective of this study was to investigate the change of $sigma_1$ receptor in the early phase of AD using [^{11}C]SA4503 PET.

Materials and methods

Subjects

We studied five patients (two men and three women, mean age ± SD, 74.6 ± 3.2 years) diagnosed as having probable AD on the basis of the National Institute of Neurological and Communicative Diseases and Stroke/Alzheimer's Disease and Related Disorders Association (NINCDS–ADRDA) criteria [25]. Magnetic resonance imaging (MRI) scans were obtained with a MAGNEX 1.5-T machine (Shimadzu, Kyoto, Japan) in the First Hospital of Nippon Medical School, and we confirmed that they had no diseases other than AD including stroke and brain tumor. To ensure the early diagnosis of AD, each patient was also examined for glucose metabolism by PET using [^{18}F]fluorodeoxyglucose ([^{18}F]FDG), and we confirmed hypometabolism of glucose in the temporoparietal lobe and posterior cingulate of all patients [26, 27]. The clinical severity of AD was scored in each patient according to the Functional Assessment of Staging [28], Mini-Mental State examination [29], and Clinical Dementia Rating [30] just before the [^{18}F]FDG PET examination.

The control group consisted of seven volunteers (two men and four women, age ± SD 62.6 ± 8.2), without any history of neurological diseases or abnormalities on physical or neurological examinations. MRI scans were obtained with a SIGNA 1.5-T machine (General Electric, WI, USA) in the Tokyo Metropolitan Geriatric Hospital for the normal subjects, and we confirmed that they had no neurological diseases, such as stroke and brain tumor. They were not currently receiving medications known to affect brain metabolism. None had a history of alcoholism.

The Ethics Committee of Tokyo Metropolitan Institute of Gerontology approved this study protocol. Informed consent in writing was obtained from all of the subjects who participated in this study.

[^{11}C]SA4503 PET

Positron emission tomography was performed in the Tokyo Metropolitan Institute of Gerontology Positron Medical Center with an SET2400 W scanner (Shimadzu, Kyoto, Japan) [31]. [^{11}C]SA4503 was prepared as described earlier [23]. The specific activity at the time of injection ranged from 23.7 GBq/μmol to 130.2 GBq/μmol (72.3 ± 34.3 GBq/μmol). The transmission data were acquired with a rotating ^{68}Ga/^{68}Ge rod source for attenuation correction. A dynamic series of decay-corrected PET data acquisition was performed in the 2D mode for 90 min starting at the time of the injection of 500 MBq of [^{11}C]SA4503. Arterial blood was sampled at 10 s, 20 s, 30 s, 40 s, 50 s, 60 s, 70 s, 80 s, 90 s, 100 s, 110 s, 120 s, 135 s, and 150 s, and at 3 min, 5 min, 7 min, 10 min, 15 min, 20 min, 30 min, 40 min, 50 min, 60 min, 75 min, and 90 min. Plasma was separated, weighed, and measured for radioactivity with an NaI (Tl) well scintillation counter. Metabolite analysis was carried out by high-performance liquid chromatography [23].

Data analysis

Image manipulations were carried out on an O2 workstation (Silicon Graphics, Mountain View, CA, USA), using a medical image processing application package "Dr. View" version 5.2 (AJS, Tokyo, Japan).

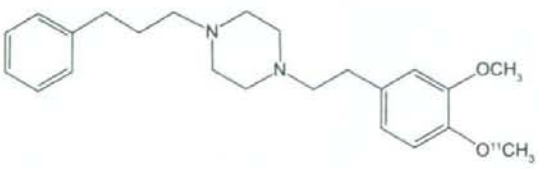

Fig. 1 Chemical structure of [^{11}C]SA4503

For [^{11}C]SA4503 PET, we generated early images for each subject by adding up the frames of the dynamic scan from 0 min to 10 min [32]. Circular regions of interest (ROIs) 10 mm in diameter and extending over two slices of the images were drawn on the cerebellum, medial temporal lobe (included hippocampus), frontal lobe, temporal lobe, occipital lobe, parietal lobe, post cingulate gyrus, thalamus, and striatum. The time course of the tissue concentration of [^{11}C]SA4503 was computed from the PET data and the interpolated ROIs throughout the scanning period. A two-tissue three-compartment model was used to estimate K_1, k_2, k_3, k_4, and the delay between metabolite-corrected plasma and tissue time activity using a Gauss–Newton algorithm [15]. The ratio of k_3 to k_4 was computed as the binding potential (BP), which is linearly related to the density of sigma$_1$ receptors. Parametric images of total distribution volume (DVt) for [^{11}C]SA4503 were also generated using a graphical analysis [33].

Statistics

Unpaired t tests were used to compare the BP in patients with AD and normal subjects. The Bonferroni correction was applied for multiple comparisons (nine comparisons corresponding to nine regions). The level of significance was set at $P < 0.05$. The statistical computation was performed using a software package "JMP" version 5.1.2 (SAS Institute, Cary, NC, USA) on a Macintosh computer.

Results

Table 1 summarizes the clinical profiles. Their average duration of illness was 2.0 ± 0.7 years. The severity of cognitive dysfunction as assessed with the Mini-Mental State examination ranged from 16 to 25.

In the ROI-based analysis, K_1 for [^{11}C]SA4503 was significantly lower in the parietal lobe of the AD patients than in that of normals, whereas there was no significant difference in other regions between AD patients and the normals (Table 2). On the other hand, BP for [^{11}C]SA4503 was significantly lower in the frontal, temporal, and occipital lobes, cerebellum and thalamus of the AD patients than in that of normals (Table 2). We also observed that BP also showed a tendency to decline in other regions of AD. Figure 2 shows representative PET images for a normal subject and a patient with AD. The DVt image demonstrates that the sigma$_1$ receptors are lower in the entire brain of the patient with AD than in that of the normal subject.

Discussion

[^{11}C]SA4503 PET demonstrated that the distribution of cortical sigma$_1$ receptors was reduced in the early phase of AD. Only in the parietal lobe could we observe a significant reduction of K_1, which was linearly related to the cerebral blood flow. The age of the control subjects was slightly younger than that of the patient group. However,

Table 1 Demographic and clinical data for patients with Alzheimer's disease (AD)

No.	Age (years)	Sex	Duration (year)	Medication before PET	FAST	MMS	CDR
1	79	M	3	Donepezil	3	25	1
2	76	M	2	Donepezil	3	21	1
3	75	F	1	Donepezil	4	16	1
4	71	F	2	None	3	17	1
5	72	F	2	None	3	22	1

PET positron emission tomography, *FAST* functional assessment of staging, *MMS* Mini-Mental State examination, *CDR* clinical dementia rating

Table 2 Comparison of K_1 and binding potential for sigma$_1$ receptors in each region in normals and patients with AD

ROI	K_1		BP	
	Normal	AD	Normal	AD
Frontal lobe	0.50 ± 0.06	0.43 ± 0.06	16.4 ± 3.0	9.2 ± 4.5*
Temporal lobe	0.52 ± 0.07	0.44 ± 0.04	17.4 ± 3.6	8.7 ± 4.3*
Hippocampus	0.46 ± 0.06	0.42 ± 0.03	18.6 ± 3.8	12.2 ± 6.8
Occipital lobe	0.58 ± 0.07	0.50 ± 0.09	13.7 ± 2.6	5.9 ± 3.3**
Parietal lobe	0.52 ± 0.06	0.39 ± 0.06*	16.7 ± 2.6	13.6 ± 10.5
Posterior cingulate	0.62 ± 0.08	0.50 ± 0.09	15.4 ± 3.2	8.7 ± 5.4
Cerebellum	0.56 ± 0.10	0.58 ± 0.06	22.5 ± 4.8	9.0 ± 5.1**
Striatum	0.55 ± 0.07	0.57 ± 0.07	13.9 ± 2.4	8.8 ± 3.5
Thalamus	0.64 ± 0.09	0.62 ± 0.09	15.2 ± 4.7	6.9 ± 2.3*

ROI regions of interest, *BP* binding potential, *AD* Alzheimer's disease
Values are mean ± SD (normal $n = 7$, AD $n = 5$).
*$P < 0.05$, **$P < 0.01$ (unpaired t test)

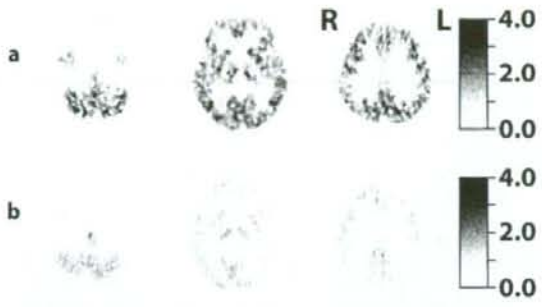

Fig. 2 Positron emission tomography (PET) images for a 65-year-old healthy woman (**a**), and a 71-year-old woman with Alzheimer's disease (**b**). Parametric images for the DVt of [^{11}C]SA4503 were generated using a graphical analysis. [^{11}C]SA4503 PET demonstrates that the sigma$_1$ receptors are widely distributed throughout the entire brain in a normal subject (**a**). In comparison with the normal subject, the number of sigma$_1$ receptors was decreased in the brain of the patient with Alzheimer's disease (**b**)

when the BP in the control subjects (62.6 ± 8.2 years) was compared with that in the young subjects (n = 9, 28 ± 4 years) reported earlier [24], it was found to be slightly decreased with aging without statistical significance (unpublished data) in spite of an age-dependent increase of the [^{11}C]SA4503 binding in rats and monkeys [14, 15]. The reduction of the BP in AD was much more marked compared with the BP in the aged control subjects. Therefore, the reduced sigma$_1$ receptor density in AD could not be derived from the slight difference in age between the control and patient groups. PET with [^{18}F]FDG and statistical image analysis applications such as statistical parametric mapping (SPM) and 3D stereotactic surface projections have shown that in patients with AD, the cerebral glucose metabolism is reduced in the temporal-, parietal-, posterior cingulate-, and prefrontal regions [26, 27]. We also confirmed a similar pattern in the present patients with AD by [^{18}F]FDG PET (data not shown). However, these findings did not correspond with the distribution of neuronal loss on postmortem studies [34]. In a [^{11}C]flumazenil PET study on AD, Ohyama et al. [35] showed that benzodiazepine receptor was less impaired than neuronal function assessed by the cerebral blood flow and glucose metabolism in the association-cortex. The benzodiazepine receptors are one of the gamma-aminobutyric acid type A ($GABA_A$) receptor complex. The present study indicated that sigma$_1$ receptors were affected from the early stages of AD, unlike $GABA_A$ receptors. Some articles showed that the sigma$_1$ receptor agonists increased extracellular acetylcholine levels in the rat frontal cortex and hippocampus [11, 12]. Increased acetylcholine does not directly affect the [^{11}C]SA4503 binding, because acetylcholine does not bind to sigma$_1$ receptors. However, reduction of the number of sigma$_1$ receptors may reflect the cholinergic system and cognitive function of patients with AD. Amyloid imaging by PET currently represents a potentially useful tool for the early diagnosis of pre-onset AD [36]. We have an interest in the relationship between sigma$_1$ receptor in the mild cognitive impairment stage and pre-onset stage of AD. Further studies will be needed using amyloid PET and [^{11}C]SA4503 PET.

The density of sigma$_1$ receptors in the cerebellum was significantly lower in AD than in normals, although K_1 in AD was comparable with that in normals. Although the cerebellum was formerly thought to be unaffected in AD, many studies have revealed cerebellar changes in AD patients [37–43]. A pathological study showed that the density of Purkinje cell was reduced in the cerebellum of AD, especially in the vermis [41]. Using glutamate as the neurotransmitter, the granule cells deliver an excitability signal to the dendrite of Purkinje cells. Chaki et al. [44] suggested that sigma$_1$ binding sites are involved in modulating the release of dopamine by interacting with *N*-methyl-D-aspartic acid (NMDA) receptors on dopaminergic nerve terminals. Release of dopamine is reduced in the putamen with Parkinson's disease, and sigma$_1$ receptors were down-regulated in the putamen with Parkinson's disease [19]. Sigma$_1$ receptors in the cerebellum may be involved in the modulation of glutamate receptor, as well as in the putamen.

Although we could observe a reduced density of sigma$_1$ receptors in the early phase of AD, we cannot say that [^{11}C]SA4503 PET is suitable for the early diagnosis of AD. We are obliged to force the subjects to remain still for over 100 min with their heads fixed in a PET machine and to cannulate their radial artery to sample the arterial blood. Most AD patients are not suitable for the protocol of [^{11}C]SA4503 PET. Prior to the examinations, we had to confirm whether each of the AD subjects in the current study could withstand the protocol of [^{11}C]SA4503 PET. Therefore, we are now investigating a shortened protocol for [^{11}C]SA4503 PET; 40- to 60-min PET scans without arterial blood sampling could possibly provide reliable results in the practical application, which will be described elsewhere.

Acknowledgments This work was supported by a Grant-in-Aid for Scientific Research (B) No. 13557077 from the Japan Society for the Promotion of Science. The authors thank Ms. M. Ando for taking care of the subjects undergoing PET scanning.

References

1. Hashimoto K, Ishiwata K. Sigma receptor ligands: possible application as therapeutic drugs and as radiopharmaceuticals. Curr Pharm Des 2006;12:3857–76.
2. Walker JM, Bowen WD, Walker FO, Matsumoto RR, De Costa B, Rice KC. Sigma receptors: biology and function. Pharmacol Rev 1990;42:355–402.
3. Quirion R, Bowen WD, Itzhak Y, Junien JL, Musacchio JM, Rothman RB, et al. A proposal for the classification of sigma binding sites. Trends Pharmacol Sci 1992;13:85–6.
4. Su TP, London ED, Jaffe JH. Steroid binding at sigma receptors suggests a link between endocrine, nervous, and immune systems. Science (New York) 1988;240:219–21.
5. Su TP. Delineating biochemical and functional properties of sigma receptors: emerging concepts. Critical Rev Neurobiol 1993;7:187–203.
6. Bowen WD. Sigma receptors: recent advances and new clinical potentials. Pharm Acta Helv 2000;7:211–8.
7. Maurice T, Urani A, Phan VL, Romieu P. The interaction between neuroactive steroids and the sigma$_1$ receptor function: behavioral consequences and therapeutic opportunities. Brain Res Rev 2001;37:116–32.
8. Hiramatsu M, Hoshino T, Kameyama T, Nabeshima T. Involvement of kappa-opioid and sigma receptors in short-term memory in mice. Eur J Pharmacol 2002;453:91–8.
9. Maurice T, Hiramatsu M, Kameyama T, Hasegawa T, Nabeshima T. Behavioral evidence for a modulating role of sigma ligands in memory processes: II. Reversion of carbon monoxide-induced amnesia. Brain Res 1994;647:57–64.
10. Senda T, Matsuno K, Okamoto K, Kobayashi T, Nakata K, Mita S. Ameliorating effect of SA4503, a novel sigma$_1$ receptor agonist, on memory impairments induced by cholinergic dysfunction in rats. Eur J Pharmacol 1996;315:1–10.
11. Matsuno K, Matsunaga K, Senda T, Mita S. Increase in extracellular acetylcholine level by sigma ligands in rat frontal cortex. J Pharmacol Exp Ther 1993;265:851–9.
12. Matsuno K, Senda T, Kobayashi T, Mita S. Involvement of sigma$_1$ receptor in (+)-N-allylnormetazocine-stimulated hippocampal cholinergic functions in rats. Brain Res 1995;690:200–6.
13. Kobayashi T, Matsuno K, Nakata K, Mita S. Enhancement of acetylcholine release by SA4503, a novel sigma$_1$ receptor agonist, in the rat brain. J Pharmacol Exp Ther 1996;279:106–13.
14. Ishiwata K, Kobayashi T, Kawamura K, Matsuno K. Age-related changes of the binding of [^{3}H]SA4503 to sigma$_1$ receptors in the rat brain. Ann Nucl Med 2003;17:73–7.
15. Kawamura K, Kimura Y, Tsukada H, Kobayashi T, Nishiyama S, Kakiuchi T, et al. An increase of sigma receptors in the aged monkey brain. Neurobiol Aging 2003;24:745–52.
16. Weissman AD, Casanova MF, Kleinman JE, London ED, De Souza EB. Selective loss of cerebral cortical sigma, but not PCP binding sites in schizophrenia. Biol Psychiatry 1991;29:41–54.
17. Matsuno K, Kobayashi T, Tanaka MK, Mita S. Sigma$_1$ receptor subtype is involved in the relief of behavioral despair in the mouse forced swimming test. Eur J Pharmacol 1996;312:267–71.
18. Lobner D, Lipton P. Sigma-ligands and non-competitive NMDA antagonists inhibit glutamate release during cerebral ischemia. Neurosci Lett 1990;117:169–74.
19. Mishina M, Ishiwata K, Ishii K, Kitamura S, Kimura Y, Kawamura K, et al. Function of sigma receptors in Parkinson's disease. Acta Neurol Scand 2005;112:103–7.
20. Jansen KL, Faull RL, Storey P, Leslie RA. Loss of sigma binding sites in the CA1 area of the anterior hippocampus in Alzheimer's disease correlates with CA1 pyramidal cell loss. Brain Res 1993;623:299–302.
21. Maurice T. Improving Alzheimer's disease-related cognitive deficits with sigma$_1$ receptor agonists. Drug News Perspect 2002;15:617–25.
22. Ishiwata K, Tsukada H, Kawamura K, Kimura Y, Nishiyama S, Kobayashi T, et al. Mapping of CNS sigma$_1$ receptors in the conscious monkey: preliminary PET study with [^{11}C]SA4503. Synapse 2001;40:235–7.
23. Kawamura K, Ishiwata K, Tajima H, Ishii S, Matsuno K, Homma Y, et al. In vivo evaluation of [^{11}C]SA4503 as a PET ligand for mapping CNS sigma$_1$ receptors. Nucl Med Biol 2000;27:255–61.
24. Sakata M, Kimura Y, Naganawa M, Oda K, Ishii K, Chihara K, et al. Mapping of human cerebral sigma$_1$ receptors using positron emission tomography and [^{11}C]SA4503. Neuroimage 2007;35:1–8.
25. McKhann G, Drachman D, Folstein M, Katzman R, Price D, Stadlan EM. Clinical diagnosis of Alzheimer's disease: report of the NINCDS-ADRDA Work Group under the auspices of Department of Health and Human Services Task Force on Alzheimer's Disease. Neurology 1984;34:939–44.
26. Herholz K, Salmon E, Perani D, Baron JC, Holthoff V, Frolich L, et al. Discrimination between Alzheimer dementia and controls by automated analysis of multicenter FDG PET. Neuroimage 2002;17:302–16.
27. Minoshima S, Giordani B, Berent S, Frey KA, Foster NL, Kuhl DE. Metabolic reduction in the posterior cingulate cortex in very early Alzheimer's disease. Ann Neurol 1997;42:85–94.
28. Reisberg B, Borenstein J, Salob SP, Ferris SH, Franssen E, Georgotas A. Behavioral symptoms in Alzheimer's disease: phenomenology and treatment. J Clin Psychiatry 1987;48 Suppl:9–15.
29. Folstein MF, Folstein SE, McHugh PR. "Mini-Mental State". A practical method for grading the cognitive state of patients for the clinician. J Psychiatr Res 1975;12:189–98.
30. Hughes CP, Berg L, Danziger WL, Coben LA, Martin RL. A new clinical scale for the staging of dementia. Br J Psychiatry 1982;140:566–72.
31. Fujiwara T, Watanuki S, Yamamoto S, Miyake M, Seo S, Itoh M, et al. Performance evaluation of a large axial field-of-view PET scanner: SET-2400 W. Ann Nucl Med 1997;11:307–13.
32. Mishina M, Senda M, Kimura Y, Toyama H, Ishiwata K, Ohyama M, et al. Intrasubject correlation between static scan and distribution volume images for [^{11}C]flumazenil PET. Ann Nucl Med 2000;14:193–8.
33. Logan J. A review of graphical methods for tracer studies and strategies to reduce bias. Nucl Med Biol 2003;30:833–44.
34. Mielke R, Schroder R, Fink GR, Kessler J, Herholz K, Heiss WD. Regional cerebral glucose metabolism and postmortem pathology in Alzheimer's disease. Acta Neuropathol (Berl) 1996;91:174–9.
35. Ohyama M, Senda M, Ishiwata K, Kitamura S, Mishina M, Ishii K, et al. Preserved benzodiazepine receptors in Alzheimer's disease measured with C-11 flumazenil PET and I-123 iomazenil SPECT in comparison with CBF. Ann Nucl Med 1999;13:309–15.
36. Nordberg A. PET imaging of amyloid in Alzheimer's disease. Lancet Neurol 2004;3:519–27.
37. Braak H, Braak E, Bohl J, Lang W. Alzheimer's disease: amyloid plaques in the cerebellum. J Neurol sci 1989;93:277–87.